

Dispersion XDM with Hybrid Functionals: Delocalization Error and Halogen Bonding in Molecular Crystals

A. Otero-de-la-Roza,^{*,†} Luc M. LeBlanc,^{*,‡} and Erin R. Johnson^{*,‡}

[†]*Departamento de Química Física y Analítica, Facultad de Química, Universidad de Oviedo, 33006 Oviedo, Spain*

[‡]*Department of Chemistry, Dalhousie University, 6274 Coburg Rd, Halifax, Nova Scotia, B3H 4R2, Canada*

E-mail: aoterodelaroza@gmail.com; luc.leblanc@dal.ca; erin.johnson@dal.ca

Abstract

The accurate calculation of relative lattice energies of molecular crystals is important in polymorph ranking and crystal structure prediction. Delocalization error has been shown to affect calculated intermolecular binding energies in DFT and is similarly expected to affect the lattice energies of some classes of molecular crystals. In this work, we explore the use of dispersion-corrected hybrid functionals in the planewave-pseudopotentials approach to reduce delocalization error. We combine several hybrid functionals with the exchange-hole dipole moment (XDM) model for dispersion and show that they generally outperform GGA functionals in the calculation of both gas-phase binding energies and molecular crystal lattice energies. We apply the resulting XDM-corrected functionals to four halogen-bonded crystals: Cl₂, Br₂, I₂, and ICl. Here, the GGA lattice energies are found to be severely overestimated due to delocalization error, while hybrid functionals successfully fix this problem. The preference of GGA functionals for monoatomic structures in the Br₂ and Cl₂ crystals is also explained. Finally, we apply a recently developed method to calculate Bader’s delocalization indices to examine the extent of intermolecular delocalization in the halogen molecular crystals. It

is shown that intermolecular delocalization indices can be used to measure the strength of halogen bonds within the crystal, as well as detect the presence of delocalization error.

Introduction

Density-functional theory (DFT) is the most popular approach for quantum-mechanical calculations in large molecules and periodic solids thanks to a favorable combination of low cost and high accuracy. Among all different variants, generalized gradient approximation (GGA) functionals¹ combined with planewave basis sets and pseudopotentials (PW/PS) are the most widely used. However, GGA functionals struggle to describe chemical reactions and present a number of additional idiosyncrasies, such as a tendency to underestimate band gaps, incorrect treatment of transition metal *d* and *f* electrons, erroneous description of intermolecular interactions, and others.^{2–4} Some of these difficulties can be alleviated by incorporating some fraction (usually 20–50%) of exact exchange.^{5,6} Hybrid functionals built in this way are standard in molecular calculations but, due to the extended nature of the basis functions, they are generally too expensive for routine use in periodic solids within the PW/PS approach. However, recent advances^{7,8} have made the use

of hybrid functionals more efficient, which has had important implications for modeling solid-state systems in which GGAs are insufficiently accurate.^{9–12}

An important shortcoming of GGAs that can be mitigated using hybrid functionals is delocalization error. Delocalization error^{3,4,13–16} arises from the failure of approximate density functionals to represent fractional-electron systems. It causes the over-stabilization of systems with fractional electron numbers,^{3,17–21} and over-estimation of the extent of charge transfer in charge-transfer complexes, among other effects.^{22–25} When modeling complexes with significant intermolecular electron delocalization, this error causes an overestimation of the binding energy. Halogen-bonded complexes^{26–28} are the paradigmatic example,^{29–31} although other interactions, such as hydrogen bonds, are also affected.³²

The relation between a functional’s performance for intermolecular interactions and its delocalization error behavior was highlighted in recent works, where we explored the use of dispersion-corrected functionals for polymorph ranking and crystal structure prediction of molecular solids.^{33,34} While relative lattice energies of molecular crystals are usually accurate enough for these purposes, there are difficulties when comparing structures featuring differing molecular conformations with varying amounts of conjugation, or when intermolecular charge transfer is present (e.g., in organic salts). In fact, delocalization error is so severe in the treatment of some neutral organic acid-base co-crystals that these materials are incorrectly predicted to exist as salts.³⁵ All these difficulties can be traced back to delocalization error from the base functional.

A characteristic of delocalization error is the systematic improvement in all affected properties when the fraction of exact exchange in the functional is increased. Given recent advances in the computational implementation of hybrid functionals for periodic solids in the PW/PS approach, a natural solution to the delocalization error problem is to build dispersion-corrected hybrid functionals.

In this article, we present the development

and first use of the exchange-hole dipole moment (XDM) dispersion model with hybrid functionals in PW/PS DFT. The interested reader is directed to Refs. 36–38 for discussion of the physics underlying the XDM approach. We determine the damping function parameters for a number of hybrid and range-separated functionals and examine the performance of the new dispersion-corrected methods for the standard X23 benchmark set of molecular crystal lattice energies.^{39,40} In addition, we examine the lattice energies and the extent of intermolecular delocalization in the Cl₂, Br₂, I₂, and ICl crystals. Halogen bonding is the principal intermolecular interaction in these crystals and it is shown that they are severely affected by delocalization error when treated with dispersion-corrected GGA functionals. We demonstrate that the XDM-corrected hybrid functionals not only resolve the difficulties experienced by their GGA counterparts for description of these halogen-bonded crystals, but also outperform GGA functionals for the treatment of intermolecular interactions in general.

Computational Methods

All PW/PS calculations used the Quantum ESPRESSO program.⁸ Two flavors of the PW/PS approach were applied: plane-wave calculations using norm-conserving pseudopotentials (NC)^{41,42} and the projector augmented wave (PAW) method.^{43,44} Both NC pseudopotentials and PAW datasets were generated for selected functionals using the `ld1.x` code included in the Quantum ESPRESSO package.

The functionals considered were the PBE,¹ BLYP,^{45,46} PW86PBE,^{1,47} and B86bPBE^{1,48} GGA functionals; the range-separated hybrid functional HSE,⁴⁹ and the PBE0,⁵⁰ B3LYP,^{6,46} and BHandHLYP^{5,46} global hybrid functionals. As B86bPBE has previously been found to give optimal performance when used in conjunction with XDM,^{51–53} we also constructed a series of global hybrid functionals based on this GGA. These functionals have an exchange-correlation

energy of the form:

$$E_{XC} = a_X E_X^{\text{HF}} + (1 - a_X) E_X^{\text{B86b}} + E_C^{\text{PBE}} \quad (1)$$

and we refer to them as B86bPBE-X. The values of the a_X parameter ranged from 0.1 to 0.5 in 0.1 increments, plus $a_X = 0.25$.

The density and wavefunction plane-wave cutoffs were determined by requiring a convergence in the B86bPBE-XDM lattice energies of the CO₂, urea, Cl₂, Br₂, and I₂ molecular crystals on the order of 0.01 kcal/mol, with and without geometry optimization. With PAW, convergence was achieved with an 80 Ry wavefunction cutoff and 800 Ry density cutoff. With NC pseudopotentials, the chosen cutoffs were 200 Ry (wavefunction) and 800 Ry (density). All hybrid calculations on molecular crystals were run using NC pseudopotentials, as the hybrid implementation in Quantum ESPRESSO fully supports only this type of pseudopotential. In order to make the calculations faster, and because equilibrium geometries do not (generally) depend very strongly on the chosen functional, all hybrid calculations were run as single points at the B86bPBE-XDM geometry. Since only single-point calculations were run, we used more lenient cutoffs: 80 Ry (wavefunction) and 320 Ry (density). This gives a convergence in the calculated lattice energies on the order 0.01–0.1 kcal/mol, which is sufficient for our purposes. Reciprocal-space k-point grids were chosen by requesting a convergence in the total energy to ≈ 0.1 mRy. We used $4 \times 4 \times 4$ k-point grids for all crystals except I₂, for which we used a $6 \times 6 \times 6$ grid. All molecular calculations were carried out in a large supercell (between 20 and 40 bohr per side, depending on the molecule) and with a single k-point at Γ .

In all cases, the exchange-hole dipole moment (XDM) dispersion correction,^{36,37,54} computed post-self-consistently, was added to the base-functional energy. All geometry relaxations were conducted using convergence thresholds of 10^{-5} Ry and 10^{-4} Ry/bohr for the energy and forces, respectively.

The crystal structures of Cl₂,⁵⁷ Br₂,⁵⁷ I₂,⁵⁸ and IC1⁵⁹ were obtained from the Crystallography Open Database (COD)⁶⁰ and are shown in

Figure 1. The unit cell parameters and atomic positions were fully relaxed with B86bPBE-XDM. We evaluated the vibrational contribution to the energy via the quasiharmonic approximation. The vibrational phonon frequencies were calculated using density-functional perturbation theory⁶¹ (DFPT) for the crystals at their equilibrium geometries and for the isolated molecules within supercells. The computed vibrational energies for the molecule ($E_{\text{vib}}^{\text{mol}}$) and the solid ($E_{\text{vib}}^{\text{sol}}$) at room temperature were used to back-correct the experimental sublimation enthalpies⁵⁵ (ΔH_{sub}):

$$\Delta E_{\text{el}} = \Delta H_{\text{sub}} - \Delta E_{\text{vib}} - \frac{7}{2} RT, \quad (2)$$

where $\Delta E_{\text{vib}} = E_{\text{vib}}^{\text{mol}} - E_{\text{vib}}^{\text{sol}}$ and ΔE_{el} is the back-corrected experimental lattice energy.

The experimental zero-pressure phases of Br₂ and I₂ (but not Cl₂) have been previously found to be dynamically unstable with dispersion-corrected GGA functionals, exhibiting imaginary vibrational modes.⁵⁶ The predicted minimum-energy structures are instead composed of infinite monoatomic chains of equidistant Br or I atoms,⁵⁶ independent of the choice of GGA functional or dispersion correction (Figure 2). To demonstrate that this may be explained by delocalization error from the GGA functionals, these alternative monoatomic phases are studied, in addition to the known experimental structures. Geometry relaxation and phonon calculations were performed for the monoatomic phases of Cl, Br, and I, using initial structures adopted from the work of George *et al.*⁵⁶ As noted above, the k-point grids were $4 \times 4 \times 4$ for Cl and Br and $6 \times 6 \times 6$ for I.

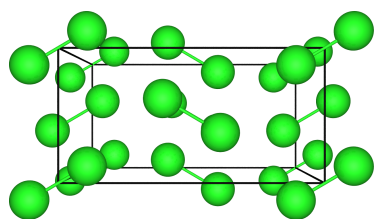
In Bader’s quantum theory of atoms in molecules (QTAIM),⁶² the average electron population of atom, N_A , is obtained by integrating the electron density, ρ , over the atomic basin:

$$N_A = \langle \hat{n}_A \rangle = \int_A \rho(\mathbf{r}) d\mathbf{r}. \quad (3)$$

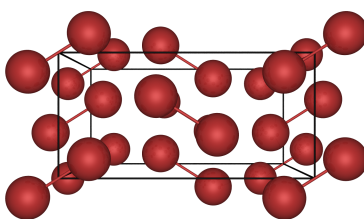
The atomic charge is given by the difference between this population and the nuclear charge:

$$q_A = Z - N_A. \quad (4)$$

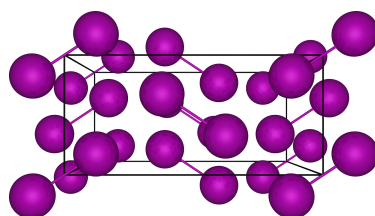
Figure 1: Unit cells of the diatomic phases of the four halogen crystals considered in this work. The experimental sublimation enthalpies at 298 K, in kcal/mol per molecule, are also given.⁵⁵



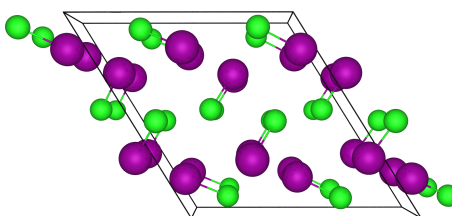
(a) Cl₂, $\Delta H_{\text{sub}} = 4.22$



(b) Br₂, $\Delta H_{\text{sub}} = 7.38$

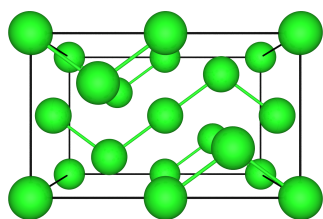


(c) I₂, $\Delta H_{\text{sub}} = 14.91$

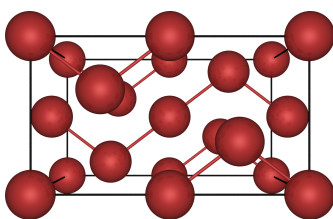


(d) ICl, $\Delta H_{\text{sub}} = 12.64$

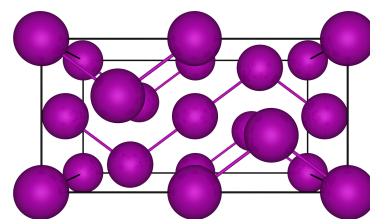
Figure 2: Monoatomic phases of the elemental halogen crystals.⁵⁶



(a) Cl



(b) Br



(c) I

Localization (λ_A) and delocalization indices (δ_{AB}) can also be defined to describe the extent of electron localization in a single atom, and electron delocalization between a pair of atoms, respectively.^{63,64} The total atomic population can then be decomposed into a sum of localization and delocalization indices:

$$N_A = \lambda_A + \frac{1}{2} \sum_{B \neq A} \delta_{AB}. \quad (5)$$

The localization index is related to the variance of the atomic population,

$$\lambda_A = N_A - \text{Var}(n_A) = \langle \hat{n}_A \rangle - (\langle \hat{n}_A^2 \rangle - \langle \hat{n}_A \rangle^2), \quad (6)$$

while the delocalization index is related to the covariance,

$$\delta_{AB} = -2\text{Cov}(n_A, n_B) = -2(\langle \hat{n}_A \hat{n}_B \rangle - \langle \hat{n}_A \rangle \langle \hat{n}_B \rangle). \quad (7)$$

Localization and delocalization indices can also be defined between whole molecules instead of atoms.⁶⁵

The Bader charges, as well as intermolecular and interatomic delocalization indices^{63,64} (DIs), were computed for all halogen crystals considered herein using our recent implementation in the Critic2 program.^{65,66} The calculation of the Wannier functions in these crystals, which is a prerequisite for the DI calculation, was carried out using the wannier90 program.⁶⁷ In addition to Bader charges and delocalization indices, we will use the total atomic and molecular delocalization (Λ), defined as:

$$\Lambda = N - \lambda \quad (8)$$

where λ is the atomic (or molecular) localization index and N is the total atomic (or molecular) electron population.⁶⁵ The value of Λ gives the number of electrons that are delocalized to (shared with) other atoms or molecules in the system. We will use Λ_M for total molecular delocalization and just Λ for total atomic delocalization.

For comparison, additional calculations using atom-centered Gaussian basis sets were performed using the CRYSTAL17 software,⁶⁸ without space-group symmetries. It is generally

quite difficult to ensure a stable self-consistent-field solution for periodic solids with large basis sets, particularly if diffuse functions are included. As such, semi-empirical methods have been developed specifically for molecular crystal applications. These have greatly reduced computational cost compared to PW/PS methods but, in general, they provide reduced accuracy in the calculated lattice energies and particularly in the crystal geometries. In this work, we employed the HF-3c method,^{69,70} which uses a minimal Gaussian basis set, and the PBEh-3c⁷¹ and HSE-3c⁷² methods, which use a polarized double-zeta basis set. In the case of HF-3c, we consider its original formulation⁶⁹ (HF-3c), as well as its scaled version for molecular crystal lattice energies^{70,73} with $s_8 = 0.6143$ and 3-body dispersion contributions included (sHF-3c). $4 \times 4 \times 4$ k-point meshes were used for all crystals (except monoatomic I and I₂, for which we used a $6 \times 6 \times 6$ grid), while non-periodic calculations were performed for the isolated molecules.

Results and Discussion

XDM parametrization and benchmarking

The two XDM damping function parameters (a_1 and a_2) for each combination of base functional and pseudopotential type (NC or PAW) used in this work are given in Table 1. The values were obtained by least-squares minimization of the mean absolute percent errors (MAPEs) in the calculated binding energies for the Kannemann-Becke set of 49 intermolecular complexes,⁷⁴ as in our previous works.^{32,54}

The MAPEs in Table 1 obtained with PAW are in good agreement with those obtained using the almost-complete aug-cc-pVTZ Gaussian basis set for the PW86PBE (11.8%) and PBE (14.3%) GGAs.³² As noted previously,³² the agreement between the PAW and Gaussian-basis results (MAPE of 9.8%) is much worse for BLYP, which may be a result of the behaviour of that functional for density tails. It is clear that there is a small penalty for using a

Table 1: XDM damping function parameters and mean absolute percent errors (MAPE) in binding energies for the KB49 set with either NC pseudopotentials or the PAW method. The exact-exchange mixing fraction (%HF) is given for each functional; for HSE, the entry of “25/0” indicates 25% short-range, and zero long-range, exact exchange.

Functional	%HF	NC			PAW		
		a_1	a_2 (Å)	MAPE	a_1	a_2 (Å)	MAPE
GGA functionals							
PBE	0	0.4283	2.4690	15.2	0.3275	2.7673	14.4
PW86PBE	0	0.7825	1.2077	12.6	0.6836	1.5045	11.7
B86bPBE	0	0.7767	1.0937	12.4	0.6512	1.4633	11.8
BLYP	0	0.6349	1.0486	11.2	0.4502	1.6210	14.8
Common hybrid functionals							
HSE	25/0	0.4206	2.4989	11.9	0.3799	2.5862	10.5
PBE0	25	0.4590	2.3581	11.1	0.4616	2.2913	7.9
B3LYP	20	0.6070	1.3862	7.4	0.6092	1.3452	8.5
BHandHLYP	50	0.2292	2.9698	10.4	0.2998	2.6953	9.3
B86bPBE-based hybrids							
B86bPBE-10X	10	0.7272	1.2674	10.8	0.6470	1.4911	10.1
B86bPBE-20X	20	0.6898	1.4072	9.6	0.6303	1.5579	8.8
B86bPBE-25X	25	0.6754	1.4651	9.2	0.6242	1.5848	8.3
B86bPBE-30X	30	0.6627	1.5181	9.0	0.6134	1.6290	7.8
B86bPBE-40X	40	0.6465	1.5981	8.9	0.5976	1.7000	7.1
B86bPBE-50X	50	0.6434	1.6405	9.1	0.5826	1.7718	6.9

plane-wave basis set and frozen cores; however, the MAPEs and damping-function parameters are consistent across different methods. The PAW damping-function parameters in Table 1 are shown for reference. The higher computational cost of PAW, together with the expense of exact exchange and the limitations of the Quantum ESPRESSO implementation, makes PAW hybrid-functional calculations impractical for molecular crystals at the moment (although PAW hybrid-functional calculations are also possible in other software codes, such as VASP^{75,76}). As such, NC pseudopotentials will be employed exclusively for hybrid calculations throughout the rest of the article.

Mirroring previous results for large Gaussian basis sets,³² the hybrid and range-separated functionals are found to outperform their GGA counterparts. Additionally, the BLYP-based functionals systematically provide greater accuracy than the PBE-based functionals for binding energies of gas-phase dimers. With NC pseudopotentials, B3LYP-XDM provides the

lowest MAPE (7.4%), but given the higher MAPE obtained with PAW for this functional, it may be a result of fortuitous error cancellation. The next best performance is obtained with the B86bPBE-based hybrids with 20-50% exact exchange, as expected. This can be justified by arguing that the asymptotic behaviour of the base B86b exchange GGA in the large-gradient limit is optimal for accurate treatment of repulsive intermolecular interactions.⁵¹⁻⁵³

The performance of the common hybrid functionals listed in Table 1, as well as B86bPBE and its 25% and 50% hybrids, was assessed for the X23 lattice energy benchmark.^{39,40} The X23 set,⁴⁰ based on our previous C21 set,³⁹ consists of 23 lattice energies for small molecular crystals that were obtained by back-correcting experimental sublimation enthalpies. This set is used to gauge the performance of different dispersion-corrected density functionals in the description of intermolecular interactions in the solid state. Mean absolute errors (MAEs) for the X23 lattice energies with the considered

methods are collected in Table 2. To place the GGA and hybrid functionals on the same footing, all calculations were performed by evaluating single-point energies at the B86bPBE-XDM equilibrium geometries. For comparison, the table also shows the results with full geometry relaxation in the GGA cases.

With the PAW method and full geometry relaxation, B86bPBE-XDM gives the best performance obtained on the X23 using a GGA method plus XDM, with an MAE of 0.85 kcal/mol.³⁷ Previous results for other GGA functionals with PAW are:³⁷ 0.88 kcal/mol (PW86PBE), 1.11 kcal/mol (PBE-XDM), and 1.31 kcal/mol (BLYP-XDM). As in the case of gas-phase dimer binding energies, we justify this by the correct behavior of its exchange enhancement factor for large reduced density gradients.^{51–53} Compared to previous results in the literature,⁷⁷ these MAEs are similar to the best-performing D3-based approaches⁷⁸ (1.1 kcal/mol (PBE-D3), 0.9 kcal/mol (TPSS-D3)) and MBD-based methods⁷⁹ (1.4 kcal/mol (PBE-MBD), 0.9 kcal/mol (PBE0-MBD)). However, it should be noted that, in the original compilation of the experimental data, Chickos⁸⁰ cites an average experimental error of 1.2 kcal/mol, so the errors obtained with the majority of these dispersion-corrected DFT methods are within the precision limit of the benchmark. All of these methods are also substantially more accurate than the original Tkatchenko-Scheffler (TS) method,⁸¹ as reported by Thomas et al.⁸² (albeit using slightly different reference data).

The calculated MAEs using NC pseudopotentials under full geometry relaxation are slightly different from the PAW results, with B86bPBE-XDM having a higher MAE, and PBE-XDM a smaller MAE, than their PAW counterparts. The difference between the NC and PAW results arise not only from the base functional part, but also from XDM, due to small differences in the implementation regarding the calculation of the XDM atomic volumes and moments. Nevertheless, the MAEs obtained with NC pseudopotentials are below 1 kcal/mol, with maximum outliers of -2.68 kcal/mol (cytosine) and -3.84 kcal/mol

(anthracene) for B86bPBE-XDM and PBE-XDM, respectively. Similarly, running the B86bPBE-XDM and PBE-XDM calculations with NC pseudopotentials and reduced plane-wave cutoffs (80 Ry, wavefunction; 320 Ry, density) at the B86bPBE-XDM/PAW equilibrium geometries also introduces small deviations with respect to the fully relaxed result, but the good performance of the two methods is preserved. This justifies running the hybrid functional calculations as single points with reduced cutoffs, which is essential in order to make the hybrid calculations feasible.

The relatively poor results for B3LYP-XDM and BHandHLYP-XDM are consistent with previous results for XDM-corrected GGAs, where BLYP-XDM gave the poorest performance for molecular crystal lattice energies,^{37,39} despite showing the best performance for the KB49 set. The B88 GGA was constructed to satisfy the correct asymptotic behaviour of the exchange Coulomb potential in the molecular density tails,⁴⁵ which are not present in crystals. The BLYP functional itself is, in fact, seldom used in periodic PW/PS calculations, with or without dispersion correction.

In general, XDM-corrected hybrid functionals outperform their GGA counterparts. In particular, PBE0-XDM and HSE-XDM both give the lowest MAE yet obtained for the X23 benchmark with XDM-corrected functionals (0.83 kcal/mol), closely followed by B86bPBE-25X-XDM. This trend is in agreement with hybrid-functional data in previous studies,^{32,83,84} where it was shown that mixing fractions of 20-25% improve the description of non-covalent interactions, as well as other thermochemical quantities such as reaction energies.^{32,83,84}

An efficient way of including exact exchange in periodic solid-state calculations is to use a Gaussian basis set instead of plane-waves. The computational cost of evaluating the exchange energy in terms of Gaussian primitive functions is greatly reduced, but the resulting methods are typically affected by basis set incompleteness error that originates from the limited number of basis functions. To this end, *ad hoc* corrections (collectively known as “3c”) have been

Table 2: Mean absolute errors (MAE) and mean errors (ME) for the X23 set of lattice energies, in kcal/mol per molecule, obtained with selected XDM-corrected functionals and NC pseudopotentials, and with semi-empirical methods using Gaussian basis sets. %HF indicates the fraction of exact exchange in the functional. full = full geometry relaxation; sp = single point at the equilibrium B86bPBE-XDM geometry.

Functional	%HF	MAE		ME	
		sp	relax	sp	relax
XDM-corrected functionals; PW/PS					
B86bPBE	0	0.92	0.94 ^a	0.03	0.19
PBE	0	1.10	0.99 ^a	-0.65	-0.49
B3LYP	20	1.29		1.05	
B86bPBE-20X	20	0.90		0.32	
HSE	25/0	0.83		0.11	
PBE0	25	0.83		0.00	
B86bPBE-25X	25	0.97		0.54	
B86bPBE-50X	50	1.10		0.84	
BHandHLYP	50	1.39		1.10	
Semi-empirical methods; Gaussian basis					
HSE-3c	42/0	1.35	1.29	0.32	0.47
PBEh-3c	42	1.23	1.47	-0.44	-0.50
HF-3c	100	2.10	1.97	0.45	1.27
sHF-3c	100	2.51	1.55	-2.19	-0.12

^a Full geometry relaxation with PAW gives MAE of 0.85 kcal/mol (B86bPBE-XDM) and 1.11 kcal/mol (PBE-XDM). ^b Full geometry relaxation with PAW gives ME of -0.21 kcal/mol (B86bPBE-XDM) and -0.76 kcal/mol (PBE-XDM).

proposed by Grimme et al. in combination with HF and a minimal basis set^{69,70} (HF-3c) and with the PBEh⁷¹ and HSE⁷² functionals using a polarized double-zeta basis set (PBEh-3c and HSE-3c). The performance of these methods for the X23 lattice energies are shown in Table 2 as well. The more expensive double-zeta basis set methods generally perform better than HF-3c, but have MAEs higher than the XDM-corrected PW/PS methods (although they are considerably cheaper than the latter). Two variants of HF-3c are shown in the table: the original version of HF-3c⁶⁹ and the “scaled” HF-3c (sHF-3c), in which some of the parameters were tweaked by fitting to the X23 reference data and 3-body dispersion terms were added.^{70,73} Naturally, the MAE of sHF-3c on the X23 is lower than plain HF-3c.

Halogen-bonded crystals

Structure and Bonding

The difficulties GGA functionals have in reproducing relative lattice energies of crystals involving delocalized molecular conformations and organic salts can be traced back to delocalization error.^{34,35} In order to test the ability of dispersion-corrected hybrid functionals to minimize this error, we focus on halogen-bonded crystals that are both simple and likely to be affected by delocalization error to a large extent. The unit cells of the four halogen crystals considered (Cl_2 , Br_2 , I_2 , and ICl) are shown in Figure 1.

The homoatomic crystals (Cl_2 , Br_2 , and I_2) all possess the same structure type. They have layers of halogen-bonded X_2 molecules in the bc plane, in which each X_2 molecule engages in four halogen bonds with its neighbors. The experimental closest intermolecular X-X distances are 3.26 (Cl), 3.29 (Br), and 3.50 Å (I), well below the sum of the corresponding van der Waals radii:⁸⁵ 3.50 (Cl), 3.70 (Br), and 3.96 Å (I), respectively. The intramolecular X-X bonds are slightly lengthened as well: 1.994 (Cl), 2.301 (Br), and 2.718 Å (I), compared to their experimental gas-phase values:⁸⁶ 1.987 (Cl), 2.281 (Br), and 2.666 Å (I). The anomalous behavior

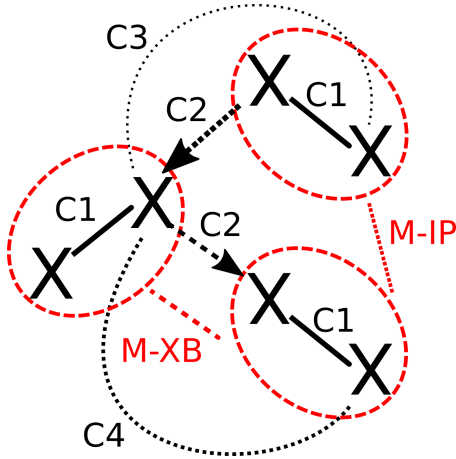
of these bond lengths under pressure has been the subject of theoretical and experimental investigation.^{87,88}

The unit cell of ICl , shown in Figure 1(d), differs from those of the other three halogen crystals. The ICl crystal has a zig-zag chain of comparatively strong halogen bonds along the c axis, as shown in the diagram associated with Table 4. Experimentally,⁵⁹ the ICl crystal has two molecules in the asymmetric unit, with bond lengths of $d(\text{C1}) = 2.437$ Å and $d(\text{C4}) = 2.368$ Å (c.f. 2.321 Å in the gas phase⁸⁶). The distances $d(\text{C2}) = 3.001$ Å and $d(\text{C3}) = 3.080$ Å are the only other two interatomic distances that are significantly lower than the corresponding sum of van der Waals radii⁸⁵ ($r_{\text{Cl}} = 1.75$ Å, $r_{\text{I}} = 1.98$ Å). This indicates the existence of halogen bonds along the zig-zag chain.

In a previous article, we showed that halogen bond strengths can be correlated with intermolecular Bader delocalization indices (DIs).²⁹ DIs indicate the number of electrons shared or delocalized between atoms or molecules in the crystal. Table 3 and Table 4 show the interatomic and intermolecular DIs calculated at the B86bPBE-XDM level in the four halogen crystals. Being a GGA, this functional typically overestimates DIs, but the results remain useful to assess the relative strengths of the different intermolecular interactions within these crystals.

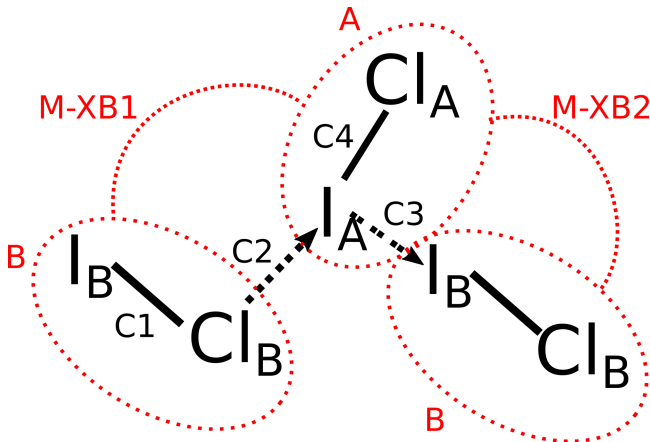
In Cl_2 , Br_2 , and I_2 , there is only one molecule in the asymmetric unit and, therefore, there is no intermolecular charge transfer. Each molecule engages in four direct halogen-bonded contacts with its immediate neighbors, as shown in the diagram beside Table 3. Both the interatomic and intermolecular DIs show an increase in the amount of delocalization for heavier atoms. The total molecular delocalization (Λ_M) goes from less than 1 for Cl_2 to around 1.8 for I_2 . For a given molecule, four of the intermolecular DIs with its immediate neighbours are equal, and much higher than the others, signifying the presence of halogen bonds (M-XB). The halogen-bonded DI is relatively modest in Cl_2 (0.209), but increases considerably in Br_2 (0.397) and in I_2 (0.503), with a

Table 3: Delocalization indices (DI) and distances (d , in Å) for the homoatomic halogen crystals (X_2) using B86bPBE-XDM at the equilibrium geometry. The diagram for interpreting the table entries is shown on the left. The arrows represent electron donation. The Mx rows give intermolecular DIs between halogen-bonded molecules (M-XB), as well as other nearest-neighbour molecules in (M-IP) or out (M-OOP) of the bc plane.



		Cl ₂	Br ₂	I ₂
Interatomic DIs and distances				
C1	DI	1.328	1.060	0.936
	d	2.029	2.411	2.837
C2	DI	0.154	0.284	0.371
	d	3.072	3.066	3.316
C3	DI	0.011	0.016	0.016
	d	4.167	4.356	4.860
C4	DI	0.038	0.091	0.109
	d	5.076	5.453	6.136
Intermolecular DIs				
M-XB	DI	0.209	0.397	0.503
M-IP	DI	0.077	0.131	0.202
M-OOP	DI	0.082	0.101	0.160
Λ_M		0.716	1.256	1.762

Table 4: Delocalization indices and distances (in Å) for the ICl crystal using B86bPBE-XDM at the equilibrium geometry. The diagram for interpreting the table entries is shown on the left. There are two non-equivalent molecules: A and B. The arrows represent electron donation. The distances and atomic delocalization indices for the four close atomic contacts (C1 to C4) are given, as well as the charge and total delocalization for the two non-equivalent atoms of each kind, the intermolecular delocalization index (through contacts C2 and C3), and the molecular charges and total delocalizations.



Interatomic distances and DIs				
	C1	C2	C3	C4
DI	0.747	0.548	0.799	1.010
d	2.601	2.741	2.901	2.428
Atomic charges and total delocalization				
	I _A	I _B	Cl _A	Cl _B
q	0.551	0.242	-0.384	-0.409
Λ	1.503	1.179	0.908	1.022
Molecular charges and DIs				
	M _A	M _B		
q	0.167	-0.167	DI(M-XB1) = 0.723	
Λ_M	1.400	1.455	DI(M-XB2) = 1.048	

delocalization in the latter that corresponds to roughly half a single bond. Despite not describing direct halogen bonds, the other intermolecular DIs also increase when moving down the halogen group. These observations point to the halogen-bonding interactions being stronger for heavier elements (as expected from their greater atomic polarizabilities); this is confirmed by the calculated lattice energies in the next section (Table 5).

The interatomic DIs in the homoatomic halogen solids reveal that the usual behavior of the intramolecular σ bonds upon halogen bond formation also happens in these crystals. The interatomic DIs corresponding to the intramolecular covalent bonds (C1 in Table 3) become smaller for stronger halogen bonds. In addition, there is a significant DI between the donor atom and the acceptor, and also between the donor and the atom behind the acceptor (C4), which is consistent with observations for the gas phase.²⁹ The DI between the acceptor atom and the atom behind the donor (C3) is comparatively much smaller and, in contrast to the other DIs, does not increase when going down the halogen group.

In ICl, there is significant intramolecular charge transfer from the iodine to the more electronegative chlorine atom, and this causes the intermolecular interactions to be more varied than in the elemental halogen crystals. The key intermolecular interactions in ICl and the calculated DIs are shown in Table 4. Within the unit cell, there are two non-equivalent molecules and, curiously, there is a significant amount of charge transfer between them. Molecule A in the diagram is cationic and molecule B is anionic, with a charge transfer of 0.167 electrons. Surprisingly, the total number of delocalized electrons is almost the same for the two molecules (1.400 for A and 1.455 for B).

In ICl, there are also two different types of halogen bonds: $\text{Cl}_B \rightarrow \text{I}_A$ and $\text{I}_A \rightarrow \text{I}_B$, where the arrow indicates electron donation. The DIs in Table 4 indicate that, as expected, the I-I halogen bond is stronger than the Cl-I halogen bond. In fact, the I-I intermolecular bond has a DI (0.799) on the order of a single covalent bond, and higher than the I-Cl bond of molecule

B (DI= 0.747), indicating that the solid has lost much of its molecular character. Being the recipient of a strong I-I halogen bond, the I-Cl in molecule B is also weaker (DI = 0.747) than in molecule A (DI = 1.010), a result that is mirrored by the calculated and experimental I-Cl bond lengths. The intermolecular DIs are significantly higher than in any of the homoatomic X_2 crystals. However, each ICl molecule engages in only two halogen bonds, rather than four, as in the case of the X_2 crystals. Since the total intermolecular DIs (1.400 and 1.455) are intermediate between the corresponding values for Br_2 and I_2 (1.256 and 1.762, respectively), we expect that the greater strength of the ICl halogen bonds roughly compensates for their reduced number, such that the lattice energy of the ICl crystal lies between that of Br_2 and I_2 . This is confirmed by our lattice energy calculations (Table 5).

Lattice energies

The performance of the XDM-corrected GGA and hybrid functionals for the lattice energies of the four halogen crystals is shown in Table 5. The calculated lattice energies are compared to the back-corrected experimental results.⁵⁵ The increase in sublimation enthalpies down the group is consistent with our previous discussion of the halogen bond strengths, as measured by the calculated DIs. Compared to the statistics for the X23 set, we see that GGAs struggle to describe the intermolecular interactions in these crystals, with extreme overbinding in all cases. The amount of overbinding is similar regardless of the GGA employed, and increases for stronger halogen bonds, which is consistent with previous results for halogen-bonded gas-phase dimers.²⁹⁻³¹

Previous work also revealed that a significant fraction of exact exchange allows dispersion-corrected functionals to describe halogen-bonded gas-phase dimers with an accuracy similar to that attained for other, less-delocalized non-covalent interactions.²⁹ Table 5 shows that this is also the case for the halogen-bonded crystals, although the optimal amount of exact exchange seems to be around 25%. This

Table 5: Computed lattice energies for halogen crystals with selected methods, in kcal/mol per molecule. Mean absolute errors (MAE) and mean errors (ME), relative to back-corrected experimental sublimation enthalpies, are also reported. The first set of XDM-corrected density functionals use planewaves and NC pseudopotentials and the second set of semi-empirical methods uses Gaussian basis sets. sp = single-point calculation at the B86bPBE-XDM geometry. opt = full geometry relaxation (with fixed space-group symmetry).

Method		Cl ₂	Br ₂	I ₂	ICl	MAE	ME
XDM-corrected functionals; PW/PS							
B86bPBE	sp	7.39	13.06	20.25	17.78	3.96	3.96
PBE	sp	8.28	13.46	21.72	18.92	4.94	4.94
B3LYP	sp	5.14	8.76	12.93	12.01	1.23	-0.95
HSE	sp	6.37	9.87	18.01	15.94	1.89	1.89
PBE0	sp	6.28	9.55	17.14	15.51	1.46	1.46
B86bPBE-25X	sp	5.84	9.09	15.46	14.36	0.69	0.52
B86bPBE-50X	sp	4.73	6.51	12.45	12.11	1.71	-1.71
BHandHLYP	sp	4.99	6.06	11.26	11.12	2.30	-2.30
Semi-empirical methods; Gaussian basis							
HSE-3c	sp	8.21	8.99	13.61	14.07	1.66	0.56
HSE-3c	opt	8.65	10.88	14.92	12.94	1.91	1.19
PBEh-3c	sp	7.40	7.45	11.42	12.19	2.21	-1.05
PBEh-3c	opt	7.84	9.81	13.68	14.55	1.87	0.81
HF-3c	sp	6.06	5.12	7.93	5.91	4.90	-4.41
HF-3c	opt	6.33	11.83	15.09	12.30	1.67	0.73
sHF-3c	sp	4.25	1.87	2.22	2.62	7.92	-7.92
sHF-3c	opt	4.91	9.17	11.33	9.66	2.35	-1.89
Experiment		5.08	8.25	15.80	13.51	—	—

is in contrast with numerous gas-phase studies of various properties affected by delocalization error, such as hydrogen-transfer energy barriers,^{32,83,84,89} charge-transfer complexes,^{22–24} ionic halogen bonds,^{29,31} and others,^{17,18} where much larger mixing fractions (near 50%) are needed to obtain accurate results.

The fact that a smaller exact-exchange fraction is needed, similar to the amount required for accurate thermochemical calculations,^{83,84} may be a consequence of the significant distortion of the intramolecular geometries in the halogen bonded crystals. Thus, they require treating molecular deformations, as well as intermolecular interactions, accurately. Another contributing factor to the disagreement with the gas-phase observations may be the use of B86bPBE-XDM equilibrium geometries for the hybrid calculations, which overstretch the intramolecular bonds in these systems. Conversely, the HSE-3c and PBEh-3c hybrid functionals give bond lengths in good agreement with experiment for the homoatomic halogens, with a maximum deviation of 0.029 Å for Cl₂; although the intramolecular bond lengths in ICl are still overestimated, by 0.042 Å and 0.075 Å for PBEh-3c and HSE-3c, respectively.

Because the incorporation of exact exchange is relatively cheap with Gaussian basis sets, we also calculated the lattice energies of the four halogen crystals using several methods recently proposed by Grimme et al. (3c) that empirically correct for basis-set incompleteness. Table 5 shows that these methods give comparable performance to many of the PW/PS hybrids, with HF-3c giving the lowest MAE (1.67 kcal/mol) if the crystal geometry is relaxed. Although far from the 0.69 kcal/mol MAE obtained with B86bPBE-25X-XDM, this is a very reasonable result, considering how inexpensive the calculation is.

However, the semi-empirical results in Table 5 also cause some concerns. Unlike for the PW/PS hybrids, the errors are not systematic, with the lattice energies for the light halogens (Cl₂ and Br₂) being overestimated and those of the heavy halogens (I₂ and ICl) being underestimated. The minimal-basis-set HF-3c gives better results than HSE-3c and PBEh-3c, which

use a larger, double-zeta polarized basis set. In addition, the scaled version of HF-3c, which was fitted to X23 reference data, and therefore typically works better for lattice energies, is worse than the original HF-3c for the halogen-bonded crystals. Perhaps more importantly, the same quantities calculated using single-point energies at the B86bPBE-XDM geometries show large errors with HF-3c (4.90 kcal/mol) and sHF-3c (7.92 kcal/mol). This is not necessarily an error from these methods, but it indicates a serious distortion relative to the B86bPBE-XDM geometries, which is not present for HSE-3c and PBEh-3c. For instance, in I₂, the HF-3c intramolecular bond lengths (C1 in Table 3) are 2.703 Å, to be compared to 2.837 Å (B86bPBE-XDM) and 2.718 Å (experiment). The HF-3c intermolecular distances are 3.871 Å (C2), compared to 3.316 Å (B86bPBE-XDM) and 3.501 Å (experiment). Therefore, the HF-3c intramolecular bonds match experiment more closely than B86bPBE-XDM, but HF-3c also severely overestimates intermolecular distances, with an I-I distance that is only slightly smaller than the sum of van der Waals radii (3.96 Å). This indicates that the good agreement between the HF-3c lattice energy for I₂ (15.09 kcal/mol) and experiment (15.80 kcal/mol) likely results from a massive error cancellation between underestimation of halogen bonding strengths with HF and overcompensation from the 3c correction terms.⁹⁰

Finally, to further confirm that the origin of the GGA lattice energy overestimation is delocalization error, we calculated the DIs at the B86bPBE-XDM equilibrium geometries of the halogen crystals for a selection of the functionals considered in this work. The halogen-bonding intermolecular DIs are shown in Table 6. The DIs all follow the same trend (Cl₂ < Br₂ < I₂ < ICl), and their interpretation is the same as in the previous discussion. In agreement with our observations for gas-phase halogen-bonded dimers,²⁹ the intermolecular DIs generally decrease with increased exact-exchange mixing and their value depends almost exclusively on the fraction of exact exchange, and not on the type of GGA upon which the hybrid is built.

Table 6: Computed intermolecular delocalization indices for the diatomic halogen crystals (halogen-bonded contact, C2 in Table 3), with selected functionals and NC pseudopotentials.

Functional	%HF	Cl ₂	Br ₂	I ₂	ICl
B86bPBE	0	0.209	0.397	0.503	1.047
PBE	0	0.209	0.398	0.504	1.046
B3LYP	20	0.179	0.354	0.471	1.008
HSE	25/0	0.175	0.359	0.477	1.016
PBE0	25	0.173	0.349	0.471	1.012
B86bPBE-25X	25	0.173	0.348	0.470	1.011
B86bPBE-50X	50	0.153	0.313	0.439	0.980
BHandHLYP	50	0.153	0.308	0.430	0.966

Competing monoatomic halogen phases

In a recent article,⁵⁶ George *et al.* noted that the experimental Br₂ and I₂ phases present imaginary phonon frequencies with several GGAs, indicating that they are not dynamically stable according to those functionals. By following the imaginary-frequency eigenvectors, crystal geometries were obtained that form monoatomic chains rather than diatomic molecules (Figure 1). This observation is problematic for the prediction of lattice energy differences of competing polymorphs with GGA functionals and it is reminiscent of similar observations about the protonation state of acid-base co-crystals,³⁵ and about bond alternation in long-chain conjugated polymers⁹¹ and hydrogen chains.⁹² In this section, we examine the source of this disagreement with experiment.

To ascertain if delocalization error is at the root of this problem, and whether hybrid functionals can be used to fix it, we performed calculations on the monoatomic phases of Cl, Br, and I. As in the case of the diatomic phases, we ran geometry relaxations with B86bPBE-XDM, then single-point calculations at the equilibrium geometry using the selected hybrid functionals. The resulting lattice energy differences between the monoatomic and diatomic phases are shown in Table 7.

Our results are consistent with the previous work of George *et al.*⁵⁶ The experimental structures of Br₂ and I₂ (but not Cl₂) have imaginary phonon modes and, as indicated in the ta-

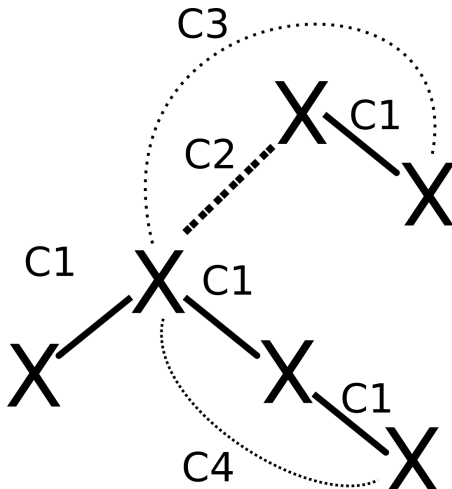
ble, the monoatomic phases of these crystals are predicted to be more stable by the B86bPBE-XDM GGA functional. George *et al.* noted that the imaginary modes can be eliminated through the use of (some) hybrid or range-separated hybrid functionals, as well as with Hartree-Fock (HF) or Møller-Plesset second-order perturbation theory (MP2).⁵⁶ In agreement with this work, our results show that the experimental form of Br₂ is favoured by all functionals except the GGAs, and HSE, which has zero exact exchange in the long-range regime. In the case of I₂, however, Table 7 shows that the monoatomic form is lower in energy for all XDM-corrected functionals considered, and an increase in the fraction of exact exchange has only a slight effect on the relative stability of both phases. George *et al.* reported that the MP2 energy difference between the two iodine phases is ~ 0.2 kcal/mol,⁵⁶ which is only marginally positive, and significantly smaller than the energy difference for the other halogen crystals.

To try to explain the disagreement with experiment for iodine, we calculated the vibrational contribution to the free energy. (This is only an estimate since the monoatomic phases of Br and I are not dynamically stable; however, the integrated phonon density of states in the imaginary frequency region is at most 0.24 out of $3 \times 8 = 24$. The phonon density of states was renormalized with the imaginary-frequency portion eliminated.) In their work, George *et al.* considered the effect of zero-point

Table 7: Lattice energy differences between the monoatomic and diatomic phases for the halogen crystals with several methods, in kcal/mol per molecule. A positive value indicates that the diatomic phase is lower in energy. The first set of XDM-corrected functionals use planewaves and NC pseudopotentials and the second set of semi-empirical method uses Gaussian basis sets. sp = single-point at the B86bPBE-XDM geometry (except MP2, which used the experimental structure for X_2 and B3LYP+D3(BJ)/def2-TZVP for the X crystals⁵⁶). opt = geometry relaxation (with fixed space-group symmetry).

Method		%HF	Cl	Br	I
XDM-corrected functionals; PW/PS					
B86bPBE	sp	0	2.24	-1.07	-0.76
PBE	sp	0	1.53	-1.28	-0.77
B3LYP	sp	20	6.43	0.23	-0.88
HSE	sp	25/0	6.64	-0.48	-0.96
PBE0	sp	25	7.24	0.10	-0.87
B86bPBE-25X	sp	25	7.36	0.21	-0.89
B86bPBE-50X	sp	50	12.85	2.02	-0.60
BHandHLYP	sp	50	13.24	2.29	-0.53
Semi-empirical methods; Gaussian basis					
HSE-3c	sp	42	8.40	2.12	-0.59
	opt	42	8.24	3.88	0.42
PBEh-3c	sp	42	9.74	2.46	-0.63
	opt	42	9.64	4.65	1.44
HF-3c	sp	100	21.97	7.81	1.29
	opt	100	22.97	14.12	7.97
sHF-3c	sp	100	22.08	7.57	1.03
	opt	100	23.43	14.55	8.51
MP2 ⁵⁶	sp			~4	~0.2

Table 8: Interatomic delocalization indices (DI) and distances (d , in Å) for the monoatomic structures of the halogen crystals (X) using B86bPBE-XDM at the equilibrium geometry. The diagram for interpreting the table entries is shown on the left (c.f. Table 3).



		Cl	Br	I
C1	DI	0.819	0.777	0.763
	d	2.286	2.570	2.946
C2	DI	0.440	0.073	0.140
	d	3.663	3.696	3.794
C3	DI	0.006	0.006	0.007
	d	4.085	4.368	4.882
C4	DI	0.201	0.204	0.186
	d	4.573	5.139	5.891

Table 9: Computed B86bPBE-XDM vibrational Helmholtz free energies (F_{vib}), and free-energy differences between the monoatomic (X) and diatomic (X_2) halogen phases. All values are given in kcal/mol per molecule (i.e. per two halogen atoms).

Crystal	$F_{\text{vib}}(X_2)$	$F_{\text{vib}}(X)$	ΔF_{vib}	ΔG
Cl	-2.38	-3.23	-0.86	1.38
Br	-3.39	-3.18	0.21	-0.86
I	-4.02	-2.89	1.13	0.37

free-energy contributions to the relative stability of I and I_2 with a GGA, and found it to be less than 0.5 kJ/mol per molecule, which is insufficient to overcome the static lattice energy difference. This is consistent with our result (in our case, 0.22 kcal/mol = 0.92 kJ/mol). However, because the atoms in these crystals are so heavy, the phonon frequencies are small and, therefore, the thermal contributions (at room temperature) are more important than the zero-point energy. Table 9 presents the vibrational Helmholtz and Gibbs free-energy differences between the diatomic and monoatomic structures for each halogen crystal. The data shows that the diatomic form is stabilized by vibrations for Br, and particularly for I, relative to the monoatomic form. In the case of iodine, I_2 is preferentially stabilized by an additional 1.13 kcal/mol from the vibrational contribution, which ensures that the diatomic structure is the thermodynamic minimum with all methods considered in this work.

Regarding the calculations using Gaussian basis sets, there is a significant difference in the relative stabilities of the monoatomic and diatomic phases between the HSE-3c and PBEh-3c methods and the HF-based methods. For Cl, all methods correctly predict Cl_2 is more stable, the single-point and fully-optimized energy differences between the phases are similar, and the magnitude of the energy difference is consistent with the planewave results. Similar observations can be made regarding the HSE-3c and PBEh-3c results for Br and I. With

these methods, the single-point energy differences are similar to the planewave results but, upon geometry optimization, the Br_2 and I_2 structures become more stable than the corresponding monoatomic phases. This result suggests that the planewave hybrid functional results are somewhat adversely affected by using the B86bPBE-XDM geometries and that, if full geometry optimizations were carried out, then I_2 would be more stable than monoatomic I, even without accounting for vibrational effects. It is also important to note that, if the geometry relaxation with Gaussian basis set methods is run without symmetry constraints, the monoatomic and diatomic initial geometries converge to the same structure (X_2) in all cases. The HF-based methods strongly prefer the X_2 structure, with a severe overestimation of the stability of Br_2 , and particularly I_2 , compared to the MP2 results. As a result of this preference, there is a significant disagreement between the single-point and fully relaxed energy differences with both HF-3c and its scaled variant.

The lattice energy results in Table 7 are reminiscent of previous observations regarding the inability of GGA functionals to predict the correct bond-length alternation and Peierls distortions in long-chain conjugated polymers^{91,93} and hydrogen chains.⁹² Both problems are related to delocalization error: GGA functionals tend to stabilize delocalized states (i.e. bond equalization) and predict too little bond alternation, while HF overstabilizes localized states and exaggerates bond alternation at the equilibrium geometry. In general, hybrid and range-separated hybrid functionals improve the description of these systems relative to GGA functionals.⁹¹⁻⁹³

The geometry and delocalization patterns in the monoatomic and diatomic phases of the halogens are similar in nature to bond-equalized and bond-alternating forms of long-chain conjugated polymers and hydrogen chains. Table 8 shows the DIs and distances in the monoatomic halogen phases (compare to Table 3 for the diatomic structures). Each atom in the monoatomic phase bonds covalently with two of its neighbors (through C1), with a DI

that is slightly lower than 1. In contrast, the DIs and distances in the corresponding diatomic phases (Table 3) show an alternation between strong covalent and weak halogen bonds. Therefore, it is to be expected that GGAs spuriously stabilize the monoatomic (bond-equalized) phase, containing two average bonds, and that HF overstabilizes the diatomic phase, with one weak and one strong bond. In the halogen crystals, the diatomic phase corresponds to the experimental structure, so HF-based methods qualitatively give the correct result, but Table 7 shows that both HF-based methods severely penalize the monoatomic phase compared to MP2.

In contrast to conjugated polymers and hydrogen chains, the picture for the halogen crystals is complicated by the fact that there are strong inter-chain halogen bonding interactions (DIs for the C2 contacts in Table 8 and Table 3). This interference from adjacent chains complicates the interpretation of the results in Table 7. While for Cl and Br the energy difference between the two phases increases with the degree of exact-exchange mixing, which is consistent with the presence of delocalization error, the same cannot be said for iodine. In this last case, MP2 predicts the monoatomic and diatomic phases to be almost equally stable, and HSE-3c and PBEh-3c relaxations favour the diatomic structure. This, together with the extreme error from HF-3c and sHF-3c compared to MP2, suggests that the slight effect of increasing the exact-exchange fraction on the monoatomic/diatomic lattice energy difference could be a consequence of using single-point energies at the B86bPBE-XDM geometry.

Summary

This work presents the first use of the XDM dispersion model in combination with hybrid functionals in the plane-wave/pseudopotentials approach. When paired with XDM, it is shown that PBE0, HSE, and a B86bPBE hybrid functional with 20% exact exchange offer significant improvement over GGAs for gas-phase dimer binding energies, as well as lattice energies of

molecular crystals. For the X23 lattice energy set, the MAEs of these three functionals are 0.83 kcal/mol (PBE0-XDM), 0.83 kcal/mol (HSE-XDM), and 0.90 kcal/mol (B86bPBE-20X-XDM).

We also explored the application of the new dispersion-corrected hybrid functionals to correct delocalization error, a problem that has been shown in previous work to be important for polymorph ranking and molecular crystal structure prediction.^{33–35} To do this, we focused on the lattice energies of four small halogen-bonded crystals: Cl₂, Br₂, I₂, and ICl. We showed that dispersion-corrected GGAs overestimate the lattice energies of the halogen crystals by ca. 30–60%, regardless of the base functional (B86bPBE or PBE). In contrast, the best hybrid functional provides excellent agreement with experimental sublimation enthalpies, with a mean absolute error of only 9%. In addition, we showed that, by taking into account vibrational effects, the spurious stability of the monoatomic phases of the Br₂ and I₂ crystals found by George et al.⁵⁶ can be explained.

To confirm that delocalization error is the at root of the difficulties GGA functionals have in treating halogen bonds, we calculated Bader’s delocalization indices in these solids using various GGA and hybrid functionals. We showed that there is significant intermolecular delocalization along halogen bonds and, in agreement with our previous results for gas-phase dimers,²⁹ the halogen-bonded intermolecular DIs depend on the amount of exact exchange that enters the functional definition, and decrease as this fraction increases.

In summary, provided their use is computationally feasible, XDM-corrected hybrid functionals are recommended for improved accuracy in lattice energies of small molecular crystals with DFT, particularly if intermolecular interactions with significant intermolecular delocalization are present.

Acknowledgements

LML and ERJ thank the Natural Sciences and Engineering Research Council of Canada

(NSERC) for financial support; LML is also grateful to the Walter C. Sumner Foundation. AOR thanks the Spanish Ministerio de Economía y Competitividad (MINECO) for a Ramón y Cajal fellowship (RyC-2016-20301) and the Spanish Ministry of Science, Innovation and Universities through the national project PGC2018-097520-A-100. All authors thank Compute Canada for computational resources.

References

- (1) Perdew, J.; Burke, K.; Ernzerhof, M. Generalized gradient approximation made simple. *Phys. Rev. Lett.* **1996**, *77*, 3865–3868.
- (2) Cohen, A. J.; Mori-Sánchez, P.; Yang, W. Challenges for density functional theory. *Chem. Rev.* **2011**, *112*, 289–320.
- (3) Cohen, A. J.; Mori-Sánchez, P.; Yang, W. Insights into Current Limitations of Density Functional Theory. *Science* **2008**, *321*, 792.
- (4) Becke, A. D. Perspective: Fifty years of density-functional theory in chemical physics. *J. Chem. Phys.* **2014**, *140*, 18A301.
- (5) Becke, A. D. A new mixing of Hartree-Fock and local density-functional theories. *J. Chem. Phys.* **1993**, *98*, 1372.
- (6) Becke, A. D. Density-functional thermochemistry. III. The role of exact exchange. *J. Chem. Phys.* **1993**, *98*, 5648–5652.
- (7) Barnes, T. A.; Kurth, T.; Carrier, P.; Wichmann, N.; Prendergast, D.; Kent, P. R. C.; Deslippe, J. Improved Treatment of Exact Exchange in Quantum ESPRESSO. *Comput. Phys. Commun.* **2017**, *214*, 52–58.
- (8) Giannozzi, P. et al. Advanced capabilities for materials modelling with Quantum ESPRESSO. *J. Phys.: Condens. Matter* **2017**, *29*, 465901.
- (9) Burke, K. Perspective on Density Functional Theory. *J. Chem. Phys.* **2012**, *136*, 150901.
- (10) Cohen, A. J.; Mori-Sánchez, P.; Yang, W. Fractional charge perspective on the band gap in density-functional theory. *Phys. Rev. B.* **2008**, *77*, 115123.
- (11) Tran, F.; Blaha, P. Accurate Band Gaps of Semiconductors and Insulators with a Semilocal Exchange-Correlation Potential. *Phys. Rev. Lett.* **2009**, *102*, 226401.
- (12) Cai, Z.-L.; Sendt, K.; Reimers, J. R. Failure of density-functional theory and time-dependent density-functional theory for large extended π systems. *J. Chem. Phys.* **2002**, *117*, 5543.
- (13) Hait, D.; Head-Gordon, M. Delocalization Errors in Density Functional Theory Are Essentially Quadratic in Fractional Occupation Number. *J. Phys. Chem. Lett.* **2018**, *9*, 6280–6288.
- (14) Kim, M.-C.; Sim, E.; Burke, K. Understanding and reducing errors in density functional calculations. *Phys. Rev. Lett.* **2013**, *111*, 073003.
- (15) Ruzsinszky, A.; Perdew, J. P.; Csonka, G. I.; Vydrov, O. A.; Scuseria, G. E. Spurious fractional charge on dissociated atoms: Pervasive and resilient self-interaction error of common density functionals. *J. Chem. Phys.* **2006**, *125*, 194112.
- (16) Lundberg, M.; Siegbahn, P. E. M. Quantifying the effects of the self-interaction error in DFT: When do the delocalized states appear? *J. Chem. Phys.* **2005**, *122*, 224103.
- (17) Johnson, E. R.; Otero-de-la-Roza, A.; Dale, S. G. Extreme density-driven delocalization error for a model solvated-electron system. *J. Chem. Phys.* **2013**, *139*, 184116.

- (18) Kim, M.-C.; Sim, E.; Burke, K. Ions in solution: Density corrected density functional theory (DC-DFT). *J. Chem. Phys.* **2014**, *140*, 18A528.
- (19) Zhang, Y.; Yang, W. A challenge for density functionals: Self-interaction error increases for systems with a noninteger number of electrons. *J. Chem. Phys.* **1998**, *109*, 2604–2608.
- (20) Grafenstein, J.; Kraka, E.; Cremer, D. The impact of the self-interaction error on the density functional theory description of dissociating radical cations: Ionic and covalent dissociation limits. *J. Chem. Phys.* **2004**, *120*, 524–539.
- (21) Vydrov, O. A.; Scuseria, G. E.; Perdew, J. P. Tests of functionals for systems with fractional electron number. *J. Chem. Phys.* **2007**, *126*, 154109.
- (22) Ruiz, E.; Salahub, D. R.; Vela, A. Charge-transfer complexes: Stringent tests for widely used density functionals. *J. Chem. Phys.* **1996**, *100*, 12265–12276.
- (23) Sini, G.; Sears, J. S.; Bredas, J. L. Evaluating the Performance of DFT Functionals in Assessing the Interaction Energy and Ground-State Charge Transfer of Donor/Acceptor Complexes: Tetrathiafulvalene-Tetracyanoquinodimethane (TTF-TCNQ) as a Model Case. *J. Chem. Theory Comput.* **2011**, *7*, 602–609.
- (24) Steinmann, S. N.; Piemontesi, C.; Delacht, A.; Corminboeuf, C. Why are the Interaction Energies of Charge-Transfer Complexes Challenging for DFT? *J. Chem. Theory Comput.* **2012**, *8*, 1629–1640.
- (25) Becke, A. D.; Dale, S. G.; Johnson, E. R. Correct Charge Transfer in CT Complexes From the Becke’05 Density Functional. *J. Chem. Phys.* **2018**, *148*, 211101.
- (26) Politzer, P.; Murray, J. S.; Clark, T. Halogen bonding: an electrostatically-driven highly directional noncovalent interaction. *Phys. Chem. Chem. Phys.* **2010**, *12*, 7754–7757.
- (27) Neaton, J. B. A direct look at halogen bonds. *Science* **2017**, *358*, 167–168.
- (28) Cavallo, G.; Metrangolo, P.; Milani, R.; Pilati, T.; Priimagi, A.; Resnati, G.; Terraneo, G. The Halogen Bond. *Chem. Rev.* **2016**, *116*, 2478–2601.
- (29) Otero-de-la-Roza, A.; Johnson, E. R.; DiLabio, G. A. Halogen bonding from dispersion-corrected density-functional theory: the role of delocalization error. *J. Chem. Theory Comput.* **2014**, *10*, 5436–5447.
- (30) Ang, S. J.; Ser, C. T.; Wong, M. W. Modeling halogen bonding with planewave density functional theory: accuracy and challenges. *J. Comput. Chem.* **2019**,
- (31) Bauzá, A.; Alkorta, I.; Frontera, A.; Elguero, J. On the Reliability of Pure and Hybrid DFT Methods for the Evaluation of Halogen, Chalcogen, and Pnictogen Bonds Involving Anionic and Neutral Electron Donors. *J. Chem. Theory Comput.* **2013**, *9*, 5201–5210.
- (32) Otero-de-la-Roza, A.; Johnson, E. R. Non-Covalent Interactions and Thermochemistry using XDM-Corrected Hybrid and Range-Separated Hybrid Density Functionals. *J. Chem. Phys.* **2013**, *138*, 204109.
- (33) Whittleton, S. R.; Otero-de-la-Roza, A.; Johnson, E. R. Exchange-Hole Dipole Dispersion Model for Accurate Energy Ranking in Molecular Crystal Structure Prediction. *J. Chem. Theory Comput.* **2017**, *13*, 441–450.
- (34) Whittleton, S. R.; Otero-de-la-Roza, A.; Johnson, E. R. Exchange-Hole Dipole Dispersion Model for Accurate Energy Ranking in Molecular Crystal Structure Prediction II: Nonplanar Molecules. *J. Chem. Theory Comput.* **2017**, *13*, 5332–5342.

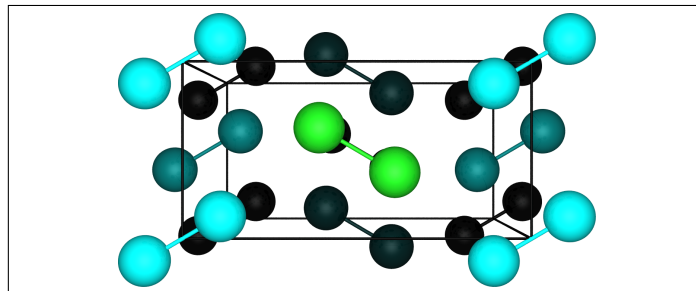
- (35) LeBlanc, L. M.; Dale, S. G.; Taylor, C. R.; Becke, A. D.; Day, G. M.; Johnson, E. R. Pervasive delocalisation error causes spurious proton transfer in organic acid-base co-crystals. *Angew. Chem. Int. Ed.* **2018**, *57*, 14906–14910.
- (36) Becke, A. D.; Johnson, E. R. Exchange-hole dipole moment and the dispersion interaction revisited. *J. Chem. Phys.* **2007**, *127*, 154108.
- (37) Johnson, E. R. In *Non-covalent Interactions in Quantum Chemistry and Physics*; Otero-de-la-Roza, A., DiLabio, G. A., Eds.; Elsevier, 2017; Chapter 5, pp 169–194.
- (38) Ayers, P. W. A perspective on the link between the exchange(-correlation) hole and dispersion forces. *J. Math. Chem.* **2009**, *46*, 86–96.
- (39) Otero-de-la-Roza, A.; Johnson, E. R. A benchmark for non-covalent interactions in solids. *J. Chem. Phys.* **2012**, *137*, 054103.
- (40) Reilly, A. M.; Tkatchenko, A. Understanding the role of vibrations, exact exchange, and many-body van der Waals interactions in the cohesive properties of molecular crystals. *J. Chem. Phys.* **2013**, *139*, 024705.
- (41) Troullier, N.; Martins, J. L. Efficient Pseudopotentials for Plane-Wave Calculations. *Phys. Rev. B* **1991**, *43*, 1993–2006.
- (42) Troullier, N.; Martins, J. L. Efficient Pseudopotentials for Plane-Wave Calculations. II. Operators for Fast Iterative Diagonalization. *Phys. Rev. B* **1991**, *43*, 8861–8869.
- (43) Blöchl, P. E. Projector Augmented-Wave Method. *Phys. Rev. B* **1994**, *50*, 17953–17979.
- (44) Kresse, G.; Joubert, D. From Ultra-soft Pseudopotentials to the Projector Augmented-Wave Method. *Phys. Rev. B* **1999**, *59*, 1758–1775.
- (45) Becke, A. D. Density-functional exchange-energy approximation with correct asymptotic behavior. *Phys. Rev. A* **1988**, *38*, 3098–3100.
- (46) Lee, C.; Yang, W.; Parr, R. G. Development of the Colle-Salvetti correlation-energy formula into a functional of the electron density. *Phys. Rev. B* **1988**, *37*, 785.
- (47) Perdew, J.; Yue, W. Accurate and simple density functional for the electronic exchange energy: Generalized gradient approximation. *Phys. Rev. B* **1986**, *33*, 8800.
- (48) Becke, A. D. On the large-gradient behavior of the density functional exchange energy. *J. Chem. Phys.* **1986**, *85*, 7184.
- (49) Krukau, A. V.; Vydrov, O. A.; Izmaylov, A. F.; Scuseria, G. E. Influence of the exchange screening parameter on the performance of screened hybrid functionals. *J. Chem. Phys.* **2006**, *125*, 224106.
- (50) Adamo, C.; Barone, V. Toward reliable density functional methods without adjustable parameters: The PBE0 model. *J. Chem. Phys.* **1999**, *110*, 6158–6170.
- (51) Lacks, D. J.; Gordon, R. G. Pair interactions of rare-gas atoms as a test of exchange-energy-density functionals in regions of large density gradients. *Phys. Rev. A* **1993**, *47*, 4681.
- (52) Zhang, Y.; Pan, W.; Yang, W. Describing van der Waals Interaction in diatomic molecules with generalized gradient approximations: The role of the exchange functional. *J. Chem. Phys.* **1997**, *107*, 7921–7925.
- (53) Kannemann, F. O.; Becke, A. D. Van der waals interactions in density-functional theory: Rare-gas diatomics. *J. Chem. Theory Comput.* **2009**, *5*, 719–727.
- (54) Otero-de-la-Roza, A.; Johnson, E. R. Van der Waals interactions in solids using the

- exchange-hole dipole moment. *J. Chem. Phys.* **2012**, *136*, 174109.
- (55) Dean, J. A. *Lange's Handbook of Chemistry, Fifteenth Edition*; McGraw-Hill, Inc., 1999.
- (56) George, J.; Reimann, C.; Deringer, V. L.; Bredow, T.; Droskowski, R. On the DFT Ground State of Crystalline Bromine and Iodine. *ChemPhysChem* **2015**, *16*, 728–732.
- (57) Powell, B. M.; Heal, K. M.; Torrie, B. H. The temperature dependence of the crystal structures of the solid halogens, bromine and chlorine Locality: synthetic Sample: at T = 5 K. *Mol. Phys.* **1984**, *53*, 929–939.
- (58) Bertolotti, F.; Shishkina, A. V.; Forni, A.; Gervasio, G.; Stash, A. I.; Tsirelson, V. G. Intermolecular Bonding Features in Solid Iodine. *Cryst. Growth Des.* **2014**, *14*, 3587–3595.
- (59) Wyckoff, R. *Crystal structures*; Interscience publishers: New York, 1960.
- (60) Grazulis, S.; Chateigner, D.; Downs, R. T.; Yokochi, A. F. T.; Quirós, M.; Lutterotti, L.; Manakova, E.; Butkus, J.; Moeck, P.; Le Bail, A. Crystallography Open Database-an open-access collection of crystal structures. *J. Appl. Cryst.* **2009**, *42*, 726–729.
- (61) Baroni, S.; De Gironcoli, S.; Dal Corso, A.; Giannozzi, P. Phonons and related crystal properties from density-functional perturbation theory. *Rev. Mod. Phys.* **2001**, *73*, 515.
- (62) Bader, R. F. W. *Atoms in Molecules. A Quantum Theory*; Oxford University Press: Oxford, 1990.
- (63) Bader, R. F.; Streitwieser, A.; Neuhaus, A.; Laidig, K. E.; Speers, P. Electron delocalization and the Fermi hole. *J. Am. Chem. Soc.* **1996**, *118*, 4959–4965.
- (64) Fradera, X.; Poater, J.; Simon, S.; Duran, M.; Solà, M. Electron-pairing analysis from localization and delocalization indices in the framework of the atoms-in-molecules theory. *Theor. Chem. Acc.* **2002**, *108*, 214–224.
- (65) Otero-de-la-Roza, A.; Pendás, A. M.; Johnson, E. R. Quantitative electron delocalization in solids from maximally localized Wannier functions. *J. Chem. Theory Comput.* **2018**, *14*, 4699–4710.
- (66) Otero-de-la-Roza, A.; Johnson, E. R.; Luña, V. Critic2: a program for real-space analysis of quantum chemical interactions in solids. *Comput. Phys. Commun.* **2014**, *185*, 1007–1018.
- (67) Mostofi, A. A.; Yates, J. R.; Lee, Y.-S.; Souza, I.; Vanderbilt, D.; Marzari, N. wannier90: A tool for obtaining maximally-localised Wannier functions. *Comput. Phys. Commun.* **2008**, *178*, 685–699.
- (68) Dovesi, R.; Erba, A.; Orlando, R.; Zicovich-Wilson, C. M.; Civalleri, B.; Maschio, L.; Rerat, M.; Casassa, S.; Baima, J.; Salustro, S.; Kirtman, B. Quantum-mechanical condensed matter simulations with CRYSTAL. *Wiley Interdiscip. Rev.: Comput. Mol. Sci.* **2018**, e1360.
- (69) Sure, R.; Grimme, S. Corrected Small Basis Set Hartree-Fock Method for Large Systems. *J. Comput. Chem.* **2013**, *34*, 1672–1685.
- (70) Brandenburg, J. G.; Grimme, S. Dispersion Corrected Hartree-Fock and Density Functional Theory for Organic Crystal Structure Prediction. *Top. Curr. Chem.* **2014**, *345*, 1–24.
- (71) Grimme, S.; Brandenburg, J. G.; Banwarth, C.; Hansen, A. Consistent Structures and Interactions by Density Functional Theory with Small Atomic Orbital Basis Sets. *J. Chem. Phys.* **2015**, *143*, 054107.

- (72) Brandenburg, J. G.; Caldeweyher, E.; Grimme, S. Screened Exchange Hybrid Density Functional for Accurate and Efficient Structures and Interaction Energies. *Phys. Chem. Chem. Phys.* **2016**, *18*, 15519–15523.
- (73) Cutini, M.; Civalleri, B.; Corno, M.; Orlando, R.; Brandenburg, J. G.; Maschio, L.; Ugliengo, P. Assessment of different quantum mechanical methods for the prediction of structure and cohesive energy of molecular crystals. *J. Chem. Theory Comput.* **2016**, *12*, 3340–3352.
- (74) Kannemann, F. O.; Becke, A. D. van der Waals interactions in density-functional theory: Intermolecular complexes. *J. Chem. Theory Comput.* **2010**, *6*, 1081–1088.
- (75) Kresse, G.; Furthmüller, J. Efficiency of ab-initio total energy calculations for metals and semiconductors using a plane-wave basis set. *Comput. Mater. Sci.* **1996**, *6*, 15.
- (76) Kresse, G.; Furthmüller, J. Efficient iterative schemes for ab initio total-energy calculations using a plane-wave basis set. *Phys. Rev. B* **1996**, *54*, 11169.
- (77) Moellmann, J.; Grimme, S. DFT-D3 study of some molecular crystals. *J. Phys. Chem. C* **2014**, *118*, 7615–7621.
- (78) Grimme, S.; Antony, J.; Ehrlich, S.; Krieg, H. A consistent and accurate ab initio parametrization of density functional dispersion correction (DFT-D) for the 94 elements H-Pu. *J. Chem. Phys.* **2010**, *132*, 154104.
- (79) Tkatchenko, A.; DiStasio, R. A.; Car, R.; Scheffler, M. Accurate and Efficient Method for Many-Body van der Waals Interactions. *Phys. Rev. Lett.* **2012**, *108*, 236402.
- (80) Chickos, J. S. Enthalpies of Sublimation after a Century of Measurement: A View as Seen Through the Eyes of a Collector. *Netsu Sokutei* **2003**, *3*, –124.
- (81) Tkatchenko, A.; Scheffler, M. Accurate molecular van der Waals interactions from ground-state electron density and free-atom reference data. *Phys. Rev. Lett.* **2009**, *102*, 073005.
- (82) Thomas, S. P.; Spackman, P. R.; Jayatilaka, D.; Spackman, M. A. Accurate lattice energies for molecular crystals from experimental crystal structures. *J. Chem. Theory Comput.* **2018**, *14*, 1614–1623.
- (83) Goerigk, L.; Grimme, S. A thorough benchmark of density functional methods for general main group thermochemistry, kinetics, and noncovalent interactions. *Phys. Chem. Chem. Phys.* **2011**, *13*, 6670–6688.
- (84) Goerigk, L.; Hansen, A.; Bauer, C.; Ehrlich, S.; Najibia, A.; Grimme, S. A look at the density functional theory zoo with the advanced GMTKN55 database for general main group thermochemistry, kinetics and noncovalent interactions. *Phys. Chem. Chem. Phys.* **2017**, *19*, 32184–32215.
- (85) Bondi, A. Van der Waals volumes and radii. *J. Phys. Chem.* **1964**, *68*, 441.
- (86) Linstrom, P. J., Mallard, W. G., Eds. *NIST chemistry webbook, NIST Standard Reference Database Number 69*; National Institute of Standards and Technology Washington, Gaithersburg MD, 20899, 2019.
- (87) Wu, M.; Tse, J. S.; Pan, Y. Anomalous bond length behavior and a new solid phase of bromine under pressure. *Sci. Rep.* **2016**, *6*, 25649.
- (88) Kenichi, T.; Kyoko, S.; Hiroshi, F.; Mitsuko, O. Modulated structure of solid iodine during its molecular dissociation under high pressure. *Nature* **2003**, *423*, 971–974.

- (89) Lynch, B. J.; Truhlar, D. G. How well can hybrid density functional methods predict transition state geometries and barrier heights? *J. Phys. Chem. A* **2001**, *105*, 2936–2941.
- (90) Kruse, H.; Grimme, S. A geometrical correction for the inter- and intra-molecular basis set superposition error in Hartree-Fock and density functional theory calculations for large systems. *J. Chem. Phys.* **2012**, *136*, 154101.
- (91) Jacquemin, D.; Femenias, A.; Chermette, H.; Ciofini, I.; Adamo, C.; André, J.-M.; Perpète, E. A. Assessment of several hybrid DFT functionals for the evaluation of bond length alternation of increasingly long oligomers. *J. Phys. Chem. A* **2006**, *110*, 5952–5959.
- (92) Zheng, X.; Liu, M.; Johnson, E. R.; Contreras-García, J.; Yang, W. Delocalization error of density-functional approximations: A distinct manifestation in hydrogen molecular chains. *J. Chem. Phys.* **2012**, *137*, 214106.
- (93) Woodcock, H. L.; Schaefer, H. F.; Schreiner, P. R. Problematic energy differences between cumulenes and polyynes: Does this point to a systematic improvement of density functional theory? *J. Phys. Chem. A* **2002**, *106*, 11923–11931.

Graphical TOC Entry



The unit-cell of the Cl_2 crystal, color-coded according to the intermolecular delocalization indices (DI). The reference molecule is shown in green; cyan indicates a higher DI and black a lower DI.